View Article Online / Journal Homepage / Table of Contents for this issue
Dynamic Article Links

Energy & Environmental Science

Cite this: *Energy Environ. Sci.*, 2012, **5**, 8553

www.rsc.org/ees

COMMUNICATION

A new electrochemical synthesis route for a BiOI electrode and its conversion to a highly efficient porous $BiVO_4$ photoanode for solar water oxidation†

Kenneth J. McDonald and Kyoung-Shin Choi*

Received 21st June 2012, Accepted 20th July 2012
DOI: 10.1039/c2ee22608a

Published on 07 August 2012. Downloaded by Pennsylvania State University on 06/03/2016 19:51:47.

A new electrodeposition condition utilizing *p*-benzoquinone reduction was developed to produce BiOI electrodes composed of extremely thin 2D BiOI crystals. These electrodes served as precursors to form porous $BiVO_4$ electrodes *via* mild chemical and thermal treatments. The resulting porous $BiVO_4$ electrodes showed outstanding photoelectrochemical performance for sulfite oxidation reaching 1.25 mA cm^{-2} at 0.5 V *vs.* RHE in 0.1 M potassium phosphate buffer (pH 7) containing 0.1 M sodium sulfite. When a *ca.* 100 nm thick FeOOH layer was deposited on the surface of $BiVO_4$ as an oxygen evolution catalyst, the kinetics of water oxidation was improved to the level of sulfite oxidation and the maximum power point for solar water oxidation was achieved at a bias as low as 0.55 V *vs.* RHE with a photocurrent density of 1.17 mA cm^{-2}. The remarkable solar water oxidation performance achieved by the porous $BiVO_4$–FeOOH system strongly encourages further morphological and compositional optimizations of the $BiVO_4$-based photoanode systems to realize highly efficient and practical solar water oxidation.

Department of Chemistry, Purdue University, West Lafayette, IN 47907, USA. E-mail: kchoi1@purdue.edu; Fax: +1-765-494-0239; Tel: +1-765-494-0049

† Electronic supplementary information (ESI) available: Detailed experimental procedures, XRD patterns of BiOI and $BiVO_4$, UV-vis spectra of $BiVO_4$ and $BiVO_4$/FeOOH, Mott–Schottky plots of $BiVO_4$, and a scheme showing how to determine P_{max} and fill factor for a solar water oxidation half reaction when a three electrode system is used. See DOI: 10.1039/c2ee22608a

Bismuth vanadate ($BiVO_4$), an n-type semiconductor, has been recently identified as a promising photoanode for use in a photoelectrochemical water splitting cell.[1–21] It has a direct bandgap of 2.4 eV and an appropriate valence band position for O_2 evolution. In addition, the conduction band of $BiVO_4$ is located very near the H_2 evolution potential, allowing the photocurrent onset to occur very near 0.0 V *vs.* RHE. This feature enables $BiVO_4$ to have an earlier photocurrent onset and generate much higher photocurrent in the low bias region than other photoanodes having a smaller bandgap but a more positive conduction band edge. When a photoanode is coupled with a photocathode in a photoelectrochemical diode assembly, an early photocurrent onset and a high fill factor are critical for achieving a high overall operating current and, therefore, a high solar-to-hydrogen conversion efficiency.[22]

Recently, the enhancement of the photocurrent of $BiVO_4$ photoanodes achieved by composition tuning and pairing with various oxygen evolution catalysts (OECs) has been reported.[5,7,8,10–20] However, most of these studies dealt with $BiVO_4$ photoanodes having relatively low surface areas. Therefore, one straightforward way to further improve the performance of $BiVO_4$ would be the introduction of high porosity to the electrode, which will increase the volume of the depletion layer and reduce electron–hole recombination. In this study, we developed a new electrochemical synthesis route to produce BiOI electrodes by exploiting the reduction of *p*-benzoquinone, the advantage of which will be elaborated below. The resulting BiOI electrodes were used as precursors to form highly porous $BiVO_4$ electrodes by mild chemical and heat treatments. The porous $BiVO_4$ electrode when combined with FeOOH as an oxygen evolution catalyst showed outstanding performance for solar water

Broader context

Among various oxide electrodes studied as photoanodes for solar water oxidation, $BiVO_4$ has shown a possibility of efficiently generating a photocurrent in the low bias region (*i.e.*, $E < 0.8$ V *vs.* RHE) as its flatband potential is located very near to the H_2 evolution potential (0.0 V *vs.* RHE). This feature is critical in achieving a high overall operating current in a p–n photoelectrochemical diode assembly. To fully exploit this advantage, a new synthesis strategy to form porous $BiVO_4$ electrodes that can minimize electron–hole recombination was developed. The resulting porous $BiVO_4$ electrode combined with an FeOOH oxygen evolution catalyst showed remarkable photoelectrochemical water oxidation performance in terms of photocurrent onset, the position of the maximum power points, fill factor, and the level of current density achieved in the low bias region. This result shows great promise to achieve efficient and practical solar water oxidation using only non-precious elements *via* simple synthesis procedures.

View Article Online

Published on 07 August 2012. Downloaded by Pennsylvania State University on 06/03/2016 19:51:47.

oxidation, achieving the maximum power point at a bias as low as 0.55 V *vs.* RHE with a photocurrent density of 1.17 mA cm^{-2}, which makes this system one of the most promising photoanodes for solar water oxidation.

The synthesis procedure used in this study is summarized in Fig. 1. The first step was the electrodeposition of BiOI electrodes by the reduction of *p*-benzoquinone to hydroquinone (eqn (1)) (Fig. 1a).[23] The plating solution was prepared by dissolving 20–40 mM $Bi(NO_3)_3$ in a solution of 400 mM KI at pH 1.75 adjusted by HNO_3. I^- serves as a complexing agent to stabilize Bi^{3+} as $[BiI_4]^-$, which otherwise is not soluble in the aqueous plating medium. 50 mM *p*-benzoquinone was added to this solution. When the *p*-benzoquinone was reduced to hydroquinone at the working electrode (WE) at −0.1 V *vs.* Ag/AgCl (4 M KCl), it consumes H^+ ions and the resulting local pH increase on the WE triggers the precipitation of crystalline BiOI on the WE, which was confirmed by X-ray diffraction (ESI, Fig. S1†). More detailed experimental procedures can be found in the ESI.†

Previously, electrodeposition utilizing local pH increase on the WE has typically used the reduction of nitrate (eqn (2)).[23,24] However, many compounds that contain metal ions having a relatively positive reduction potential such as BiOI containing Bi^{3+} could not be electrochemically produced using nitrate reduction because metal ions present in the plating solution are reduced to metal before nitrate reduction occurs (*e.g.*, Bi^{3+} to Bi^0, eqn (3)).[22] In this study, we exploited the electrochemical reduction of *p*-benzoquinone, which has a much more positive reduction potential (eqn (1)) than Bi^{3+}, to make the electrodeposition of BiOI possible. There has been one study on using *p*-benzoquinone reduction for the deposition of a biopolymer, chitosan,[25] but this is the first demonstration of utilizing benzoquinone reduction for inorganic materials synthesis, which will significantly expand the scope of electrochemical materials synthesis.

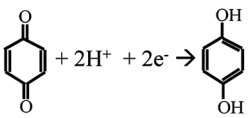

$$E^\circ = 0.699\ \text{V} \qquad (1)$$

$$NO_3^- + H_2O + 2e^- \rightarrow NO_2^- + 2OH^-,\ E^\circ = 0.01\ \text{V} \qquad (2)$$

$$Bi^{3+} + 3e^- \rightarrow Bi^0,\ E^\circ = 0.308\ \text{V} \qquad (3)$$

The second step was the conversion of BiOI to $BiVO_4$, which was achieved by adding a 30% NH_4OH solution containing 100 mM V_2O_5 on the BiOI surface and annealing in air at 520 °C for 6 h

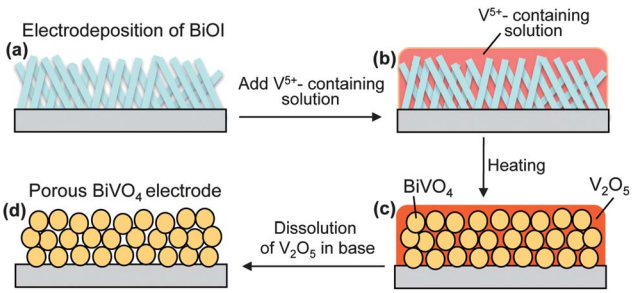

Fig. 1 Schematic representation of the procedures used to prepare porous $BiVO_4$ electrodes.

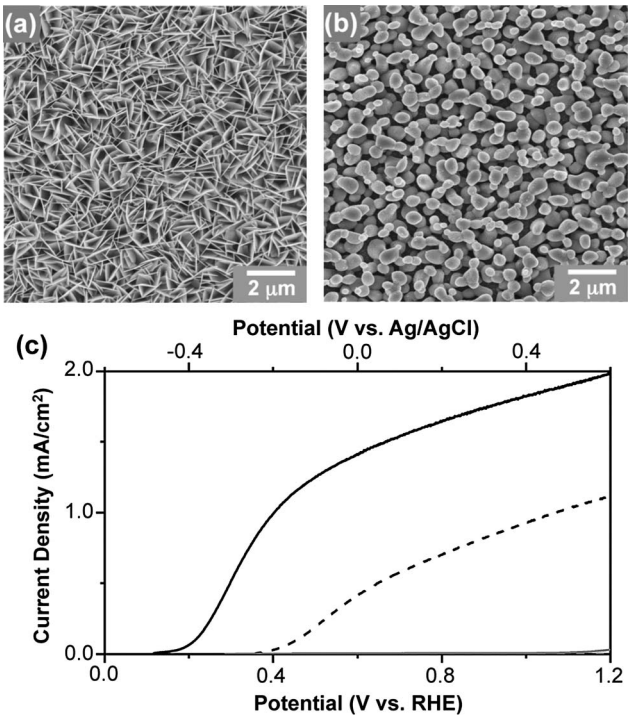

Fig. 2 SEM images of (a) BiOI and (b) $BiVO_4$ electrodes; (c) photocurrent density–potential curve of $BiVO_4$ electrodes in 0.1 M phosphate buffer (pH 7) before (---) and after (—) adding 0.1 M sulfite (AM 1.5G, 100 mW cm^{-2} illumination). Dark currents are shown as gray lines.

(Fig. 1b and c). The annealing procedure resulted in the decomposition of BiOI into Bi_2O_3 and I_2, which sublimes. Then Bi_2O_3 reacted with V_2O_5 to form $BiVO_4$. Due to the excess amount of V^{5+} ions in the solution added, the resulting film contained amorphous V_2O_5 as an impurity phase, which was removed by soaking the electrode in a 1 M NaOH solution for 20 min while stirring (Fig. 1d). After the soaking process, energy dispersive spectroscopy confirmed that the Bi : V ratio of the electrode is 1 : 1 and no iodide is present in the film. XRD shows peaks from only the $BiVO_4$ phase having a monoclinic scheelite structure (JCPDS# 14-0688), confirming the absence of other crystalline impurity phases (ESI, Fig. S1†).

The SEM images of BiOI and $BiVO_4$ are shown in Fig. 2a and b, which demonstrate the advantage of producing $BiVO_4$ by the conversion of the electrochemically produced BiOI electrode. The BiOI electrode is composed of extremely thin two-dimensional (2D) plate-like crystals, which reflects the atomic level crystal structure of BiOI composed of 2D BiOI layers. During thermal annealing procedure, each 2D plate of BiOI was converted and contracted to a round particle of $BiVO_4$ having a 3D crystal structure, creating sub-micron scale voids between the particles. The discrete 2D plate morphologies of BiOI crystals with ample space between them appear to effectively limit the grain growth and the final grain size of $BiVO_4$ particles, resulting in the formation of porous $BiVO_4$ electrodes.

The photocurrent density–potential curve of $BiVO_4$ electrodes was measured under AM 1.5G (100 mW cm^{-2}) illumination in 0.1 M potassium phosphate buffer (pH 7) (Fig. 2c). The $BiVO_4$ electrode produced an anodic photocurrent confirming the n-type nature of $BiVO_4$. However, the amount of the photocurrent generated for water oxidation was not impressive and also the photocurrent onset potential (0.35 V *vs.* RHE) was shifted considerably in the positive

 This journal is © The Royal Society of Chemistry 2012

View Article Online

Published on 07 August 2012. Downloaded by Pennsylvania State University on 06/03/2016 19:51:47.

direction from its flatband potential determined from the Mott–Schottky plots (*ca.* −0.05 V *vs.* RHE) (ESI, Fig. S2†). In order to determine whether the poor catalytic nature of the $BiVO_4$ surface for O_2 evolution serves as a limiting factor for photocurrent generation, 0.1 M sodium sulfite was added to the electrolyte. Oxidation of sulfite ($SO_3^{2-}/SO_3^{\cdot-}$, $E^\circ = 0.73$ V *vs.* NHE; $SO_3^{2-}/S_2O_6^{2-}$, $E^\circ = 0.026$ V *vs.* NHE), is thermodynamically and kinetically much more favourable than water oxidation.[26] Therefore, surface recombination losses due to slow interfacial hole transfer kinetics can be assumed negligible for photo-oxidation of sulfite. Indeed, when sulfite was present in the electrolyte, a remarkable increase in the photocurrent was observed, reaching 1.25 mA cm^{-2} at 0.5 V *vs.* RHE. This result clearly indicated that the slow interfacial kinetics for O_2 evolution played a role in suppressing the photocurrent of $BiVO_4$ for water oxidation.

The photocurrent generated by the porous $BiVO_4$ for sulfite oxidation is much higher than that by the recently reported non-porous $BiVO_4$ electrode, which was prepared by annealing electrochemically produced amorphous Bi–V–O films.[19] For example, the non-porous $BiVO_4$ electrode generated a photocurrent of 0.73 mA cm^{-2} at 0.5 V *vs.* RHE when the photocurrent–potential characteristics were obtained using the identical condition. However, the porous $BiVO_4$ electrode generated a photocurrent of 1.25 mA cm^{-2} at 0.5 V *vs.* RHE, indicating *ca.* 70% photocurrent improvement. The flatband potential values for the non-porous and porous $BiVO_4$ electrodes obtained from Mott–Schottky plots (ESI, Fig. S2†) are comparable,[19] suggesting that the observed performance difference is not due to the difference in carrier density or flatband potential but mainly due to the increase in the surface area, thereby increasing the volume of the depletion layer and reducing electron–hole recombination.

The early photocurrent onset (0.21 V *vs.* RHE) and remarkably high photocurrent generated by the porous $BiVO_4$ electrode in the low bias region for sulfite oxidation are very encouraging because they suggest that a similar level of photocurrent may be achieved for water oxidation if an appropriate oxygen evolution catalyst (OEC) is placed on the $BiVO_4$ surface. To probe this possibility, FeOOH that was recently identified as a good OEC to couple with $BiVO_4$ was conformally coated on the $BiVO_4$ electrode by photodeposition.[19]

Photodeposition of FeOOH was carried out by back-side illumination of $BiVO_4$ electrodes with an intensity of 1.6 mW cm^{-2} for 1 h in a 0.1 M $FeCl_2$ (pH 4) solution while stirring. The photodeposition is based on utilizing photogenerated holes in $BiVO_4$ to oxidize Fe(II) ions to Fe(III) ions (eqn (4)).[27,28] Fe(III) ions are insoluble in an aqueous medium ($[Fe^{3+}] = \sim 10^{-7}$ at pH = 4.1) and precipitate out as FeOOH on the $BiVO_4$ film (eqn (5)).[27,28] A constant potential of +0.27 V *vs.* Ag/AgCl (4 M KCl) was applied during photodeposition to increase the photodeposition rate. (This potential is not enough to electrodeposit FeOOH.)

$$Fe^{2+} \rightarrow Fe^{3+} + e^-, \; E^\circ = 0.771 \text{ V} \quad (4)$$

$$Fe^{3+} + 2H_2O \rightarrow FeOOH + 3H^+, \; \log[Fe^{3+}] = 4.84 - 3 \text{ pH} \quad (5)$$

Since photodeposition utilizes photogenerated holes in $BiVO_4$ to oxidize Fe(II) to Fe(III), FeOOH by photodeposition was formed only on the $BiVO_4$ surface. Therefore, in order to ensure that any bare FTO substrate exposed between the $BiVO_4$ particles was covered by FeOOH, additional electrodeposition of FeOOH was carried out by applying +1.2 V *vs.* Ag/AgCl (4 M KCl) for 10 min in the same solution after photodeposition. Exposure of the bare FTO surface to the electrolyte may leak photoexcited electrons to the electrolyte before they reach the counter electrode, decreasing the overall photocurrent. Both the photodeposition time and electrodeposition time of FeOOH reported here were optimized to maximize the photocurrent generated by $BiVO_4$/FeOOH electrodes for O_2 evolution.

Top and side view SEM images of the FeOOH layers deposited on $BiVO_4$ electrodes are shown in Fig. 3a and b. The top view SEM image shows that the catalyst uniformly covers the surface of the $BiVO_4$ electrode while maintaining the porosity between the $BiVO_4$ particles. The side view SEM image clearly shows the conformal nature of the *ca.* 100 nm thick FeOOH coating on individual $BiVO_4$ particles.

The photocurrent for water oxidation in 0.1 M potassium phosphate buffer generated by a $BiVO_4$/FeOOH photoanode is shown in Fig. 3c. The presence of FeOOH greatly improved the photocurrent for water oxidation such that it became very close to the level of photocurrent generated for sulfite oxidation by the $BiVO_4$ electrode (Fig. 2c). However, the photocurrent for water oxidation by the $BiVO_4$/FeOOH photoanode is still lower than the photocurrent for sulfite oxidation by the $BiVO_4$ photoanode, indicating that a portion of the holes that reach the surface of the $BiVO_4$/FeOOH photoanode were lost by surface recombination during water oxidation.

Due to the early photocurrent onset (0.21 V *vs.* RHE) and an outstanding fill factor of the photocurrent profile, the maximum power point (P_{max}) for water oxidation was achieved at 0.55 V *vs.* RHE with a photocurrent density of 1.17 mA cm^{-2}. (See ESI,

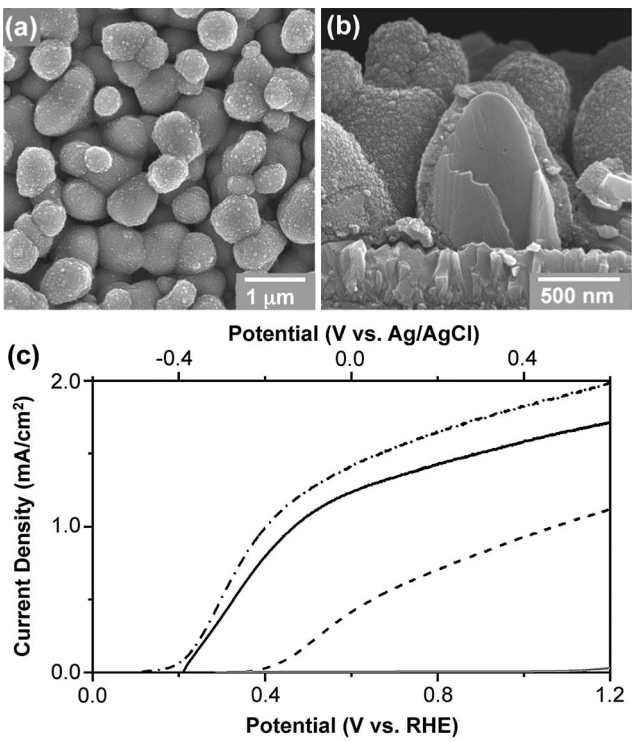

Fig. 3 (a) Top view and (b) side view SEM images of $BiVO_4$/FeOOH photoanode; (c) photocurrent density–potential curve of $BiVO_4$/FeOOH photoanode in 0.1 M phosphate buffer (pH 7) (—). Dark current is shown as a gray line. For easy comparison, photocurrent density–potential curves of bare $BiVO_4$ photoanode for water oxidation (---) and sulfite oxidation (-·-) shown in Fig. 2c are also included (AM 1.5G, 100 mW cm^{-2} illumination).

View Article Online

Published on 07 August 2012. Downloaded by Pennsylvania State University on 06/03/2016 19:51:47.

Fig. S3† for the determination of P_{max} and fill factor for a solar water oxidation half reaction when a three electrode system is used.)[22] The fact that the P_{max} is achieved at a bias as low as 0.55 V *vs.* RHE and the photocurrent density obtained at 0.55 V *vs.* RHE is as high as 1.17 mA cm^{-2} makes the porous $BiVO_4$/FeOOH electrode one of the best oxide-based photoanode systems reported to date. The outstanding performance of $BiVO_4$/FeOOH demonstrated in this study was possible owing to the combination of the very negative flatband potential of $BiVO_4$, the porous structure of $BiVO_4$ minimizing electron–hole recombination, and FeOOH being able to improve the water oxidation kinetics considerably.

The performance shown in Fig. 3c is the average performance of our $BiVO_4$/FeOOH systems, which is significantly improved from the average performance of the previously reported non-porous $BiVO_4$/FeOOH electrodes.[19] For example, photocurrent densities achieved at 0.55 V *vs.* RHE in the photocurrent–potential characteristics are 1.17 mA cm^{-2} and 0.82 mA cm^{-2} for an average porous $BiVO_4$/FeOOH and an average non-porous $BiVO_4$/FeOOH, respectively. However, the performance difference observed for water oxidation between porous and non-porous $BiVO_4$ electrodes was less than the performance difference observed for sulfite oxidation.[19] This is because unlike sulfite oxidation, the increase in electron–hole separation achieved by the porous structure is not fully utilized to increase the photocurrent for water oxidation in the porous $BiVO_4$/FeOOH electrode. Improving the quality of the $BiVO_4$/FeOOH junction and identifying a more efficient OEC that can better interface with the $BiVO_4$ surface are under investigation in order to completely suppress surface recombination losses and maximize photocurrent for water oxidation.

When the $BiVO_4$/FeOOH electrode was used for sulfite oxidation and was compared with the performance of the bare $BiVO_4$ for sulfite oxidation, no improvement in the photocurrent was observed. This indicates that although FeOOH itself is a semiconductor having a bandgap of *ca.* 2.1 eV (ESI Fig. S2†),[19,27] it does not play a role in enhancing photon absorption or electron–hole separation in the case of sulfite oxidation. Therefore, the enhancement in the photocurrent for water oxidation achieved by $BiVO_4$/FeOOH is due to FeOOH mainly serving as an oxygen evolution catalyst.

The stability of the $BiVO_4$/FeOOH photoanode was tested by monitoring the photocurrent density change over time while applying a constant potential of 0.5 V *vs.* RHE. Fig. 4(a) shows that the steady state photocurrent of *ca.* 0.9 mA cm^{-2} was maintained for six hours without noticeable decay. The fluctuation of the photocurrent observed in the plot is due to O_2 bubbles collected on the electrode surface interfering with photocurrent generation and also due to our attempts to manually remove the O_2 bubbles by shaking the electrode or the electrolyte, which also resulted in a slight change in the distance between the electrode and the light source (or the volume of electrolyte between them). The inset of Fig. 4(a) shows that when $BiVO_4$ is not coupled with FeOOH, the initial photocurrent decays quickly to a significantly lower steady state photocurrent due to the poor catalytic nature of $BiVO_4$ for water oxidation.

In order to confirm that the photocurrent generated by $BiVO_4$/FeOOH at 0.5 V *vs.* RHE using 100 mW cm^{-2} AM 1.5G illumination was truly associated with water oxidation, O_2 detection measurement was carried out during photoelectrolysis of water. The photocurrent-to-O_2 conversion efficiency was calculated by comparing the amount of O_2 calculated from the photocurrent assuming 100% Faradaic efficiency and the actual amount of O_2 produced during photoelectrolysis, which was measured by a fluorescence-based O_2 sensor. The result shows that 95% of photocurrent was used for O_2 production (Fig. 4b). The remaining 5% of photocurrent may be due to experimental errors associated with the precision of the O_2 sensor (*ca.* ±5%) or the photocurrent associated with photocorrosion occurring at the pinholes where FeOOH is not completely covering the $BiVO_4$ surface. No visible sign of photocorrosion in our $BiVO_4$/FeOOH electrodes was observed after several hours of photoelectrolysis operation, but photocorrosion of bare $BiVO_4$ used for water oxidation without a good OEC has been well noted in the literature.[1,6,19]

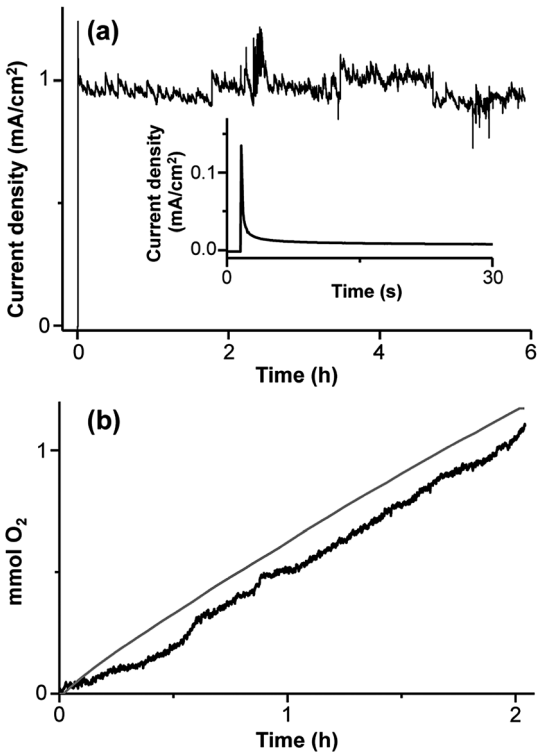

Fig. 4 (a) Photocurrent of $BiVO_4$ (inset) and $BiVO_4$/FeOOH photoanode measured at 0.5 V *vs.* RHE in 0.1 M phosphate buffer (pH 7); (b) the amount of O_2 calculated from the photocurrent assuming 100% Faradaic conversion efficiency (gray line) and the amount of O_2 actually detected (black line) when $BiVO_4$/FeOOH photoelectrode operates at 0.5 V *vs.* RHE in 0.1 M phosphate buffer (pH 7). For both (a) and (b) AM 1.5G, 100 mW cm^{-2} illumination was used.

In summary, we have developed a new cathodic electrodeposition condition to prepare crystalline BiOI electrodes using *p*-benzoquinone reduction. The polycrystalline BiOI electrode composed of extremely thin 2D plates allowed for the preparation of porous $BiVO_4$ photoanodes using a simple chemical and thermal treatment. The resulting porous $BiVO_4$ electrodes showed remarkable photoelectrochemical performance for sulfite oxidation and also for water oxidation when combined with FeOOH OEC. For solar water oxidation, the $BiVO_4$/FeOOH photoanode achieved the P_{max} point at 0.55 V *vs.* RHE with a photocurrent density of 1.17 mA cm^{-2}. The outstanding and stable solar water oxidation performance achieved by the $BiVO_4$/FeOOH system composed of only non-precious elements prepared by simple synthesis procedures warrants further optimization studies on morphologies and compositions of the $BiVO_4$-based photoanodes.

 This journal is © The Royal Society of Chemistry 2012

View Article Online

Acknowledgements

This work was supported by the Division of Chemical Sciences, Geosciences, and Biosciences, Office of Basic Energy Sciences of the U.S. Department of Energy through Grant DE-FG02-05ER15752 and made use of the Life Science Microscopy Facility at Purdue University.

References

1 K. Sayama, A. Nomura, Z. G. Zou, R. Abe, Y. Abe and H. Arakawa, *Chem. Commun.*, 2003, 2908.
2 A. Iwase and A. Kudo, *J. Mater. Chem.*, 2010, **20**, 7536.
3 W. J. Luo, Z. Q. Wang, L. J. Wan, Z. S. Li, T. Yu and Z. G. Zou, *J. Phys. D: Appl. Phys.*, 2010, **43**, 7.
4 G. C. Xi and J. H. Ye, *Chem. Commun.*, 2010, **46**, 1893.
5 H. Ye, J. Lee, J. S. Jang and A. J. Bard, *J. Phys. Chem. C*, 2010, **114**, 13322.
6 S. P. Berglund, D. W. Flaherty, N. T. Hahn, A. J. Bard and C. B. Mullins, *J. Phys. Chem. C*, 2011, **115**, 3794.
7 T. H. Jeon, W. Choi and H. Park, *Phys. Chem. Chem. Phys.*, 2011, **13**, 21392.
8 W. J. Luo, Z. S. Yang, Z. S. Li, J. Y. Zhang, J. G. Liu, Z. Y. Zhao, Z. Q. Wang, S. C. Yan, T. Yu and Z. G. Zou, *Energy Environ. Sci.*, 2011, **4**, 4046.
9 N. Myung, S. Ham, S. Choi, Y. Chae, W. G. Kim, Y. J. Jeon, K. J. Paeng, W. Chanmanee, N. R. de Tacconi and K. Rajeshwar, *J. Phys. Chem. C*, 2011, **115**, 7793.
10 H. S. Park, K. E. Kweon, H. Ye, E. Paek, G. S. Hwang and A. J. Bard, *J. Phys. Chem. C*, 2005, **115**, 17870.
11 S. K. Pilli, T. E. Furtak, L. D. Brown, T. G. Deutsch, J. A. Turner and A. M. Herring, *Energy Environ. Sci.*, 2011, **4**, 5028.
12 H. Ye, H. S. Park and A. J. Bard, *J. Phys. Chem. C*, 2011, **115**, 12464.
13 D. K. Zhong, S. Choi and D. R. Gamelin, *J. Am. Chem. Soc.*, 2011, **133**, 18370.
14 F. F. Abdi and R. van de Krol, *J. Phys. Chem. C*, 2012, **116**, 9398.
15 S. P. Berglund, A. J. E. Rettie, S. Hoang and C. B. Mullins, *Phys. Chem. Chem. Phys.*, 2012, **14**, 7065.
16 W. J. Jo, J. W. Jang, K. J. Kong, H. J. Kang, J. Y. Kim, H. Jun, K. P. S. Parmar and J. S. Lee, *Angew. Chem., Int. Ed.*, 2012, **51**, 3147.
17 W. J. Luo, Z. S. Li, T. Yu and Z. G. Zou, *J. Phys. Chem. C*, 2012, **116**, 5076.
18 S. K. Pilli, T. G. Deutsch, T. E. Furtak, J. A. Turner, L. D. Brown and A. M. Herring, *Phys. Chem. Chem. Phys.*, 2012, **14**, 7032.
19 J. A. Seabold and K.-S. Choi, *J. Am. Chem. Soc.*, 2012, **134**, 2186.
20 D. E. Wang, R. G. Li, J. Zhu, J. Y. Shi, J. F. Han, X. Zong and C. Li, *J. Phys. Chem. C*, 2012, **116**, 5082.
21 S. J. Hong, S. Lee, J. S. Jang and J. S. Lee, *Energy Environ. Sci.*, 2011, **4**, 1781–1787.
22 M. G. Walter, E. L. Warren, J. R. McKone, S. W. Boettcher, Q. X. Mi, E. A. Santori and N. S. Lewis, *Chem. Rev.*, 2012, **110**, 6446.
23 *CRC Handbook of Chemistry and Physics*, ed. D. R. Lide, CRC Press: Boca Raton, FL, 92nd edn, 2011–2012, ch. 8, pp. 20–29.
24 G. H. A. Therese and P. V. Kamath, *Chem. Mater.*, 2000, **12**, 1195.
25 Q. M. Zhou, Q. J. Xie, Y. C. Fu, Z. H. Su, X. Jia and S. Z. Yao, *J. Phys. Chem. B*, 2007, **111**, 11276.
26 (*a*) R. Sarala, M. A. Islam, S. B. Rabin and D. M. Stanbury, *Inorg. Chem.*, 1990, **29**, 1133; (*b*) T. Hemmingsen, *Electrochim. Acta*, 1992, **37**, 2775.
27 R. L. Spray and K.-S. Choi, *Chem. Mater.*, 2009, **21**, 3701.
28 *Atlas of Electrochemical Equilibria in Aqueous Solutions*, ed. M. Pourbaix, National Association of Corrosion Engineers, Houston, 2nd edn, 1974, p. 384.

Published on 07 August 2012. Downloaded by Pennsylvania State University on 06/03/2016 19:51:47.